

CHARGED PARTICLE MULTIPLICITY IN PROTON–LEAD COLLISIONS AT $\sqrt{s_{NN}} = 5.02$ TeV IN THE ATLAS EXPERIMENT*

BARTŁOMIEJ ŻABIŃSKI

on behalf of the ATLAS Collaboration

The Henryk Niewodniczański Institute of Nuclear Physics PAN
Radzikowskiego 152, 31-342 Kraków, Poland

(Received April 17, 2014)

This note describes ATLAS results on multiplicity of produced charged particles in p +Pb collisions at the centre-of-mass energy of 5.02 TeV. The charged particle density was measured in a wide pseudorapidity range as a function of the collision centrality using 2.1 million events which were collected during a “pilot run” in September 2012. Analysis methods, centrality determination and the particle production dependence on the number of nucleons participating in the collisions are presented.

DOI:10.5506/APhysPolB.45.1653

PACS numbers: 25.75.-q, 25.75.Ag

1. Introduction

Since 2010, the $p + p$, Pb+Pb and p +Pb collisions at the highest centre-of-mass energies were delivered by the Large Hadron Collider (LHC) [1] and measured using the ATLAS detector [2] giving a chance to observe new phenomena. While analysis of $p + p$ collisions is focused predominantly on the searches for the Higgs boson and signs of a new physics beyond the Standard Model, the studies of Pb+Pb collisions are aimed at investigation of properties of the Quark–Gluon Plasma (QGP). The charged particle multiplicity in heavy ion collisions is one of the most important global observables characterizing properties of the matter created in nuclear collisions. It has been studied at lower than LHC energies in many experiments using beams interacting with a fixed target [3–5] or delivered in collider accelerators [6–8] for various colliding systems. In the analysis of $A+A$ collisions, properties of the QGP thermalization and collective evolution are obscured by purely nuclear

* Presented at the Cracow Epiphany Conference on the Physics at the LHC, Kraków, Poland, January 8–10, 2014.

effects. These latter phenomena can be studied in $p + A$ collisions [9], where formation of the QGP is not expected. The measurement of charge particle multiplicity as a function of centrality of collisions can show how multiple interactions of a proton in a heavy nucleus affect bulk particle production. Such measurements provide valuable tests of saturation models and nuclear parton distributions.

In September 2012, the LHC provided first $p + \text{Pb}$ collisions at the centre-of-mass energy $\sqrt{s_{NN}} = 5.02$ TeV. Due to the difference between proton and lead beam energies, the collisions have a rapidity boost of -0.47 with respect to the ATLAS detector frame of reference. In this pilot run, the beam with the lead nuclei had positive rapidity (Pb-going side) and the proton beam had negative rapidity (proton-going side)¹. During this short run, ATLAS collected 2.1 million minimum-bias events corresponding to an estimated integrated luminosity of $1 \mu\text{b}^{-1}$.

2. The ATLAS detector and experimental setup

The ATLAS detector [2] is the largest detector at the LHC accelerator. In its structure we can distinguish three main layers of subdetectors: tracking system, calorimeters and muon chambers. For the presented here analysis, the innermost part of the ATLAS tracking system: silicon Pixel detector [2] is the most important. It is placed very closely to the beam pipe and consists of the “barrel” and “endcap” sections. In the barrel part, rectangular silicon modules are arranged in three layers with the first of them at 50.5 mm from the beam axis. The two endcaps, located on both sides of the barrel, consist of silicon modules forming three rings. The Pixel detector covers over 5 pseudorapidity units in the central rapidity region.

In the centrality determination signals from the forward calorimeter (FCal) are used. This detector covers $3.1 < |\eta| < 4.9$ range, but only the part at positive η measuring Pb nucleus fragmentation is used in the centrality calculations. The trigger for minimum-bias $p + \text{Pb}$ collisions is based on information from the Minimum-Bias Trigger Scintillators (MBTS) which consists of two rings with 16 scintillator modules each, placed at positive and negative z and covering $2.1 < |\eta| < 3.9$.

3. Event selection

The primary trigger requires effectively at least one signal on each side of the MBTS detector, with the time difference between them less than 10 ns. The standard track reconstruction algorithm, optimized for $p + p$ minimum-bias events, was used to reconstruct tracks and find collision vertices [10].

¹ In the ATLAS coordinates frame, z axis is along the beam direction, x axis is horizontal and points towards the centre of the LHC ring, and y axis is vertical.

The collision vertex range was restricted to $|z_{\text{vtx}}| < 175$ mm. The contribution from pileup was small and was further suppressed by rejecting events with two or more reconstructed vertices that are separated in z by more than 15 mm, reducing the pileup fraction to about 10^{-4} [11]. In p +Pb collisions, significant contributions from electromagnetic and diffractive processes are expected. Some fraction of them is rejected by trigger requirements but, in addition, a rapidity gap analysis was applied to remove the remaining events of these classes. In this analysis, the detector is divided into slices of $\Delta\eta = 0.2$ and each slice containing at least one reconstructed track or a calorimeter cluster with $p_T > 200$ MeV was treated as occupied. The edge-gaps are calculated as a distance in pseudorapidity between the edge of the calorimeter (-4.9 or 4.9) and the nearest occupied slice. Events with large edge-gaps on positive η direction $\Delta\eta_{\text{gap}}^{\text{Pb}} > 2.0$ are excluded from the analysis, as they represent predominantly electromagnetic processes or diffractive excitations of the proton.

4. Centrality estimation

To determinate centrality of p +Pb collisions, the total transverse energy from forward calorimeter on the Pb-going side, ΣE_T^{Pb} , was used. The signals in the FCal were evaluated at the electromagnetic energy scale and have not been corrected for hadronic response. The transverse energy from FCal on the Pb-going side is more sensitive measure of the collision centrality (as expected to be associated with multiple interactions of the proton in the target nucleus) than the summed transverse energy from FCal on the proton-going side ΣE_T^p or the sum from both sides.

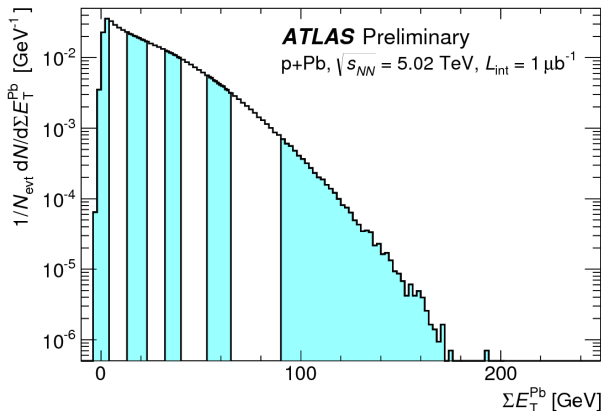


Fig. 1. Distribution of the summed transverse energy deposited on the lead-going side, ΣE_T^{Pb} . The distribution is divided into nine intervals which correspond to centrality classes, from most central events (large ΣE_T^{Pb}) to peripheral collisions (small ΣE_T^{Pb}) [11].

Figure 1 presents distribution of ΣE_T^{Pb} after applied events selection criteria. The alternating shaded and unshaded bands represent centrality intervals which are defined in terms of percentiles of the ΣE_T^{Pb} distribution after accounting for an estimated inefficiency of $2 \pm 2\%$ for $p+\text{Pb}$ events.

The following centrality intervals are used in this analysis: 0–1%, 1–5%, 5–10%, 10–20%, 20–30%, 30–40%, 40–60%, 60–90%. The most peripheral collisions were excluded from the analysis due to uncertainties regarding event selection efficiency and remaining contributions of electromagnetic or diffractive events.

5. Measurement of charged particle multiplicity

In the presented analysis, three different reconstruction methods, based on the information from the Pixel detector, were used [11]. In the first two methods, a tracklet reconstruction algorithm [12–14] is applied. The two-point tracklet is defined by the reconstructed vertex and two clusters registered in two different layers of the Pixel detector. For each pair of clusters, the first from *layer* 0 closest to the beam pipe and second from more distant *layer* 1 (or *layer* 2) the difference in their positions in η and ϕ were calculated

$$\Delta\eta = \eta_1 - \eta_0, \quad \Delta\phi = \phi_1 - \phi_0. \quad (1)$$

Using Monte Carlo simulations of events obtained from the HIJING generator [15], the optimal selection criteria reducing the false cluster combinations were estimated. The minimal values of the differences $|\Delta\phi|$ and $|\Delta\eta|$ are 0.1 and 0.015 respectively.

Two variants of the tracklet method were used. Both of them require one cluster in the innermost layer but differ in the treatment of the second cluster. In the first approach, “Method 1”, clusters from farther layer in the search region are treated as one hit. This way the number of fake tracklets is significantly reduced. In the second approach, “Method 2”, all combination of clusters in the search region are used to form tracklets. Later, the combinatoric background is removed by subtracting the distribution of tracklets obtained from modified events in which clusters from the outer layers are flipped in the azimuthal angle (in this case only fake tracklets are reconstructed). Both methods are schematically illustrated in Fig. 2.

In addition to the two tracklet methods, the third method based on pixel tracks was used. The pixel tracks are found by the standard ATLAS track reconstruction algorithm, but restricted to the Pixel detector. The combinatoric background is in this case suppressed even more than in “Method 1”, but the acceptance is smaller than in other two methods due to inactive areas in the Pixel detector.

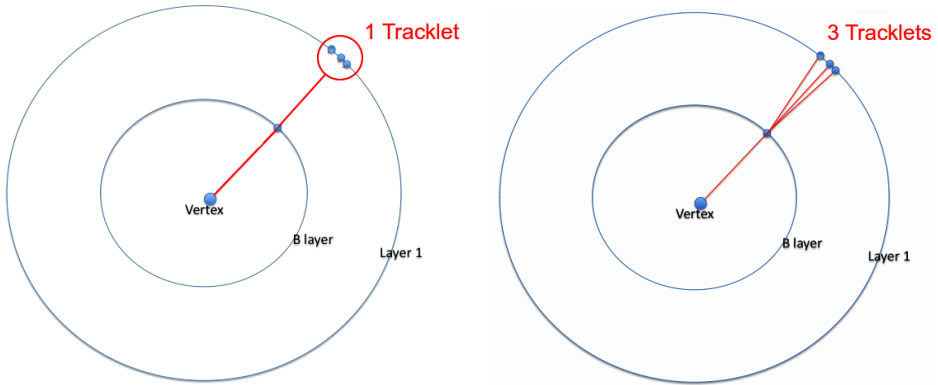


Fig. 2. Schematic picture of tracklet “Method 1” (left-hand side) and “Method 2” (right-hand side).

For each reconstruction method the corrections factors, C , were determined, as described below, and then applied to the data. The left panel of Fig. 3 shows the pseudorapidity distribution for the generated primary charged particles from HIJING [15] and reconstructed η distributions for tracklets and pixel tracks. Using these distributions, the correction factors are evaluated as

$$C(O, z_{\text{vtx}}, \eta) \equiv \frac{N_{\text{pr}}(O, z_{\text{vtx}}, \eta)}{N_{\text{rec}}(O, z_{\text{vtx}}, \eta)}, \quad (2)$$

where N_{pr} is the number of generated primary charged particles and N_{rec} is the number of tracklets or tracks reconstructed with the considered methods. The correction factors are evaluated as a function of occupancy, O , position of the event vertex z_{vtx} and η in 8 intervals of detector occupancy and 7 intervals of vertex position. These corrections account for several effects such as inactive areas in the Pixel detector, reconstruction efficiency, contributions from fake tracklets or tracks and secondary particles, losses due to tracks or tracklets selection cuts *etc.* The final charged particle pseudorapidity density is calculated as

$$\frac{dN_{\text{ch}}}{d\eta} = \frac{1}{N_{\text{evt}}} \sum_{z_{\text{vtx}}} \frac{\Delta N^{\text{raw}}(O, z_{\text{vtx}}, \eta) C(O, z_{\text{vtx}}, \eta)}{\Delta \eta}, \quad (3)$$

where N_{evt} is the number of events, ΔN^{raw} indicates either the number of reconstructed tracklets or pixel tracks in the data. Right panel in Fig. 3 shows experimental distributions from three methods, both the raw distributions of tracklets or tracks and final results after applying corrections. The corrected charged particle densities are in good agreement for all three methods, what indicates that the correction procedure is well understood.

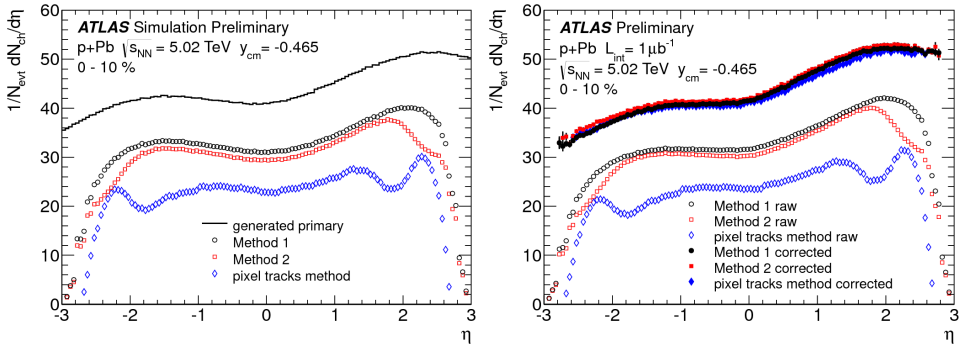


Fig. 3. Charged particle multiplicity in 0–10% most central events as a function of pseudorapidity obtained for generated primary charged particles (black histogram), from two tracklet methods (circles and squares) and from the pixel Track method (diamonds). In the left panel results obtained for Monte Carlo simulations (raw tracklets and tracks distributions) are shown, while in the right panel results obtained from experimental data: raw tracklets and tracks distributions and the final corrected particle density (full symbols) are included [11].

In the following, the “Method 1” is used for the measurement of $dN_{\text{ch}}/d\eta$. “Method 2” is used for estimation of systematic uncertainties and the pixel track method serves as a cross check.

The total systematic uncertainties are largest for peripheral events, where they reach 5.8% in the barrel and 7.5% in the endcaps, while for central collisions they are 3% in the barrel and 5.4% in the endcaps.

6. Results

The $dN_{\text{ch}}/d\eta$ measurement is presented in Fig. 4, where the charged particle density measured in pseudorapidity range from -2.7 to 2.7 for eight centrality classes is shown. The charged particle density increases with centrality, and in more central collisions we observe asymmetric distributions due to enhanced particle production in the lead-going side. In the most peripheral events, the charged particle density becomes similar to the charged particle density in $p + p$ collisions [10, 16].

In order to study the centrality evolution of particle production, the distributions of the charged particle density measured in different centrality classes are divided by the charged particle density for the most peripheral event class (60–90%). The ratios are shown in Fig. 5. The original double peak structure disappears, the ratios increase approximately linearly with pseudorapidity with the slope of this dependence growing with centrality.

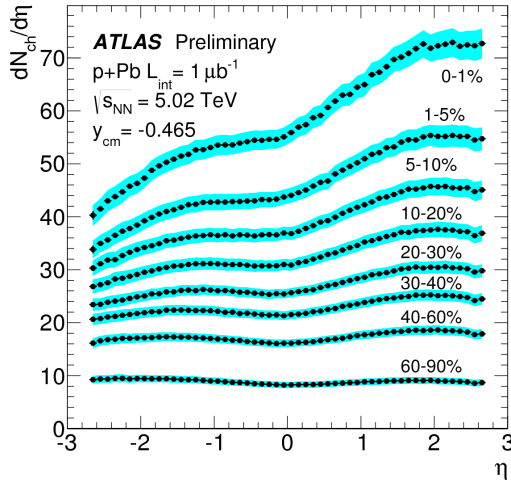


Fig. 4. Charged particle density in $p + Pb$ collisions at $\sqrt{s_{NN}} = 5.02$ TeV as a function of pseudorapidity obtained for eight centrality classes. Shaded bands represent systematic uncertainties [11].

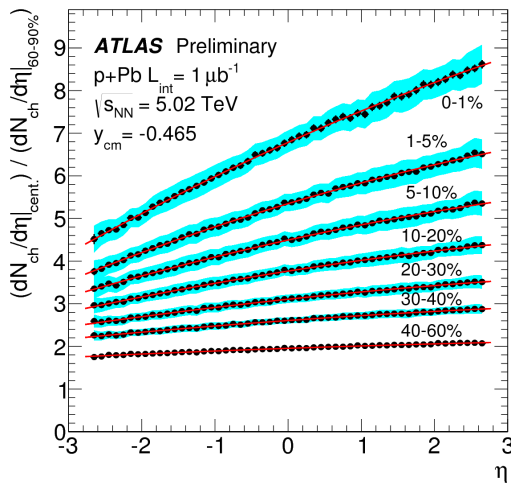


Fig. 5. Charged particle density for seven centrality intervals divided by the charged particle density for the most peripheral events. Solid/red lines represent second order polynomials fitted to the ratios [11].

For the most central collisions, this ratio at $\eta = 2.7$ is almost two times higher than for $\eta = -2.7$. The ratios in Fig. 5 are fitted with a second order polynomial and parameters of this function are presented in Table I.

TABLE I

Parameters of the second order polynomial fits ($a\eta^2 + b\eta + c$) to ratios of $dN_{\text{ch}}/d\eta$ distributions in different centrality classes divided by the $dN_{\text{ch}}/d\eta$ distribution for the most peripheral collisions (60–90%) [11].

Centrality ratio	a	b	c
0–1%/60–90%	-0.033 ± 0.006	0.77 ± 0.05	6.78 ± 0.28
1–5%/60–90%	-0.030 ± 0.005	0.515 ± 0.031	5.35 ± 0.22
5–10%/60–90%	-0.0218 ± 0.0035	0.377 ± 0.021	4.49 ± 0.18
10–20%/60–90%	-0.0169 ± 0.0025	0.269 ± 0.014	3.77 ± 0.14
20–30%/60–90%	-0.0113 ± 0.0020	0.182 ± 0.010	3.11 ± 0.11
30–40%/60–90%	-0.0076 ± 0.0016	0.122 ± 0.006	2.61 ± 0.08
40–60%/60–90%	-0.0037 ± 0.0011	0.0595 ± 0.0031	1.95 ± 0.06

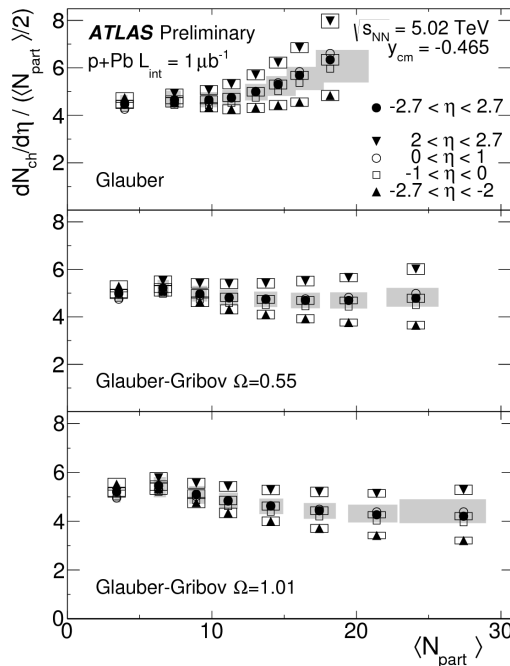


Fig. 6. Charged particle density divided by the number of pairs of participants as a function of $\langle N_{\text{part}} \rangle$ for three implementations of the Glauber model and in several η intervals. Standard Glauber model implementation is shown in the top panel. In the middle and in the bottom panel, the Glauber–Gribov implementations with $\Omega = 0.55$ and $\Omega = 1.01$, respectively, are presented. The shaded boxes represent the total systematic uncertainty [11].

An important characteristic of the particle production is the multiplicity of charged particles per a pair of nucleons participating in the collision, N_{part} . The estimate of $\langle N_{\text{part}} \rangle$ requires modelling of the interactions of nucleons in the nuclei, which is commonly provided by the Glauber model. In this analysis, the number of participants is obtained from three different versions of the Glauber model. In Fig. 6 the charged particle multiplicity divided by the mean number of participant pairs, in several pseudorapidity intervals, is shown as a function of the number of participants N_{part} . For the standard Glauber model [17], in the top panel we observe an increase of the normalized charged particle density starting from $N_{\text{part}} = 10$. This behaviour was not expected and it may mean that the standard Glauber method does not work well at LHC energies. Plots in Fig. 6 present the same dependence but for N_{part} calculated using two versions of the Glauber–Gribov model [18, 19] with different values of the Ω parameter, which represents the width of the assumed fluctuations of the nucleon–nucleon cross section, σ_{NN} . In these cases, we observe different behaviours indicating sensitivity to the initial-state modelling.

7. Conclusions

The charged particle density in p +Pb collisions was measured by the ATLAS experiment. The measurement was done in $|\eta| < 2.7$ range and for the 90% most central collisions. Centrality of collisions was estimated using information from the forward calorimeter on Pb-going side. The average number of participants $\langle N_{\text{part}} \rangle$ was obtained with the Monte Carlo Glauber, and Glauber–Gribov models for each centrality interval. The shape of $dN_{\text{ch}}/d\eta$ distribution changes with centrality. In the most peripheral collisions, this shape is approximately symmetric but with growing centrality of collisions it becomes increasingly asymmetric. On the other hand, the ratio of $dN_{\text{ch}}/d\eta$ divided by $dN_{\text{ch}}/d\eta$ in the most peripheral collisions (60–90%) is approximately linear in η . The slope of this ratio strongly depends on centrality. Charged particle density is sensitive to the modelling of the initial-state, especially in the most central collisions.

This work was supported in part by the National Science Center grant DEC-2013/08/M/ST2/00320 and by PL-Grid Infrastructure.

REFERENCES

- [1] L. Evans, P. Bryant (Eds.), *JINST* **3**, S08001 (2008).
- [2] ATLAS Collaboration, *JINST* **3**, S08003 (2008).
- [3] W. Busza, R. Ledoux, *Annu. Rev. Nucl. Part. Sci.* **38**, 119 (1988).

- [4] J. Elis *et al.*, *Phys. Rev.* **D22**, 13 (1980).
- [5] C. De Marzo *et al.* [Bari–Cracow–Liverpool–Munich–Nijmegen Collaboration], *Phys. Rev.* **D26**, 1019 (1982).
- [6] PHOBOS Collaboration, *Phys. Rev. Lett.* **93**, 082301 (2004).
- [7] ALICE Collaboration, *Phys. Rev. Lett.* **110**, 082302 (2013).
- [8] ATLAS Collaboration, *Phys. Lett.* **B710**, 363 (2012).
- [9] L.P. Cserani, J. Kapusta, L.D. McLerran, *Phys. Rev. Lett.* **97**, 152303 (2006).
- [10] ATLAS Collaboration, *New J. Phys.* **13**, 053033 (2011).
- [11] ATLAS Collaboration, ATLAS-CONF-2013-096, <http://cds.cern.ch/record/1599773>
- [12] ATLAS Collaboration, *Phys. Lett.* **B710**, 363 (2012).
- [13] PHENIX Collaboration, *Phys. Rev. Lett.* **86**, 3500 (2015).
- [14] PHOBOS Collaboration, *Phys. Rev.* **C83**, 024913 (2011).
- [15] X.-N. Wang, M. Gyulassy, *Phys. Rev.* **D44**, 3501 (1991).
- [16] ATLAS Collaboration, *Phys. Lett.* **B688**, 21 (2010).
- [17] M.L. Miller, K. Reygers, S.J. Sanders, P. Steinberg, *Annu. Rev. Nucl. Part. Sci.* **57**, 205 (2007).
- [18] V. Guzey, M. Strikman, *Phys. Lett.* **B633**, 245 (2006).
- [19] M. Avioli, M. Strikman, *Phys. Lett.* **B722**, 347 (2013).